Super-Adsorbent Hydrogels for Removal of Methylene Blue from Aqueous Solution: Dye Adsorption Isotherms, Kinetics, and Thermodynamic Properties

Buddhabhushan Salunkhe and Thomas P. Schuman *

Chemistry, Missouri University of Science and Technology, Rolla, MO 65409, USA; bps7z7@mst.edu
* Correspondence: tschuman@mst.edu; Tel.: +1-(573)-341-6236

Abstract: Removal of dyes through adsorption from wastewater has gained substantial interest in recent years, especially in development of hydrogel based adsorbents, owing to their easy use and economical nature. The aim of the present study was to design a super-adsorbent hydrogel based on sodium styrenesulfonate (NaSS) monomer for removal of dyes like methylene blue (MB). NaSS displays both an aromatic ring and strongly ionic group in its monomer structure that can enhance adsorption capacity. Poly(sodium styrenesulfonate-co-dimethylacrylamide) hydrogels were prepared by solution free radical polymerization using gelatin methacryloyl (GelMA) as crosslinker, creating a highly porous, three-dimensionally crosslinked polymer network contributing to higher swelling ratios of up to 27,500%. These super-adsorbent hydrogels exhibited high adsorption capacity of 1270 mg/g for MB adsorption with above 98% removal efficiency. This is the first report for such a high adsorption capacity for dye absorbance for NaSS-based hydrogels. Additionally, the adsorption kinetics using a pseudo-first-order and the Freundlich adsorption isotherm models for multilayer, heterogeneous adsorption processes has been reported. The adsorbents' reusability was confirmed through 4 repeated cycles of desorption-adsorption. The results discussed herein illustrate that NaSS based chemistries can be used as an efficient option for removal of organic dyes from contaminated wastewater.

Keywords: super-adsorbent hydrogels; methylene blue; adsorption; kinetic; isotherm

1. Introduction

Organic dyes are chemical compounds that are widely used in industries such as textile [1,2], paper, leather tanning [3], plastics [4], coatings [5,6], pharmaceutical [7], cosmetics [8], printing, ground water tracing, and many other chemical industries [9–13]. These industries consume large amounts of water at different stages and the wastewater generated is discharged as polluted effluents, which contain toxic substances such as heavy metals ions, dyes and other organic pollutants. The effluents cause serious environmental pollution and pose threats to human health as the pollutants are non-biodegradable, highly toxic, and often carcinogenic and/or mutagenic in nature [14]. Due to toxic effects of dyes, their removal from wastewater has become an important aspect in the field of water remediation. Among a variety of organic dyes, methylene blue (MB) is the most commonly used dye in textile and paper industries [15]. MB is toxic in nature with a carcinogenic and mutagenic character and is readily dissolved in the water. MB is harmful to humans at a lower dosage of 1 to 7.5 ppm [16] and can cause increased heart rate, jaundice, vomiting, shock, eye burns and mental confusion.

A variety of methods are employed for removal of these dyes that include chemical oxidation [17], photochemistry [18], biological treatments, adsorption [12,19,20], ion exchange [21], and physical treatments [12]. Among these treatments, adsorption is among the most promising technique for dye removal from wastewater and has attracted interests

of researchers and industry owing to its advantages like simple design, low cost, insensitivity to pollutants, easy regeneration, and effectiveness [22]. Hydrogels are most widely studied material as an adsorbent for organic dye removal from wastewater owing to their excellent water absorption, high porosity, easy handling, and facile preparation resulting in a flexible network of polymer chains that helps penetration of solutes into the network [23]. The polymer backbone in these hydrogels can be designed with specific hydrophilic functional groups, e.g., carboxylic acids, amines, or sulfonic acids, which could be employed as complexing agents for dyes possessing opposite charge [15,24–26]. Hydrogels have physically well-defined, three-dimensional structures and can swell to several times of their original volume in aqueous solutions, creating a very large surface contact area for adsorption of these organic dyes [19,27].

In last decade, engineered hydrogels have emerged as an effective adsorbent for removal of a wide range of dyes from wastewater [20,28]. Some recent examples that utilize engineering materials such as graphene [29], carbon nanotubes [30,31], activated charcoal [32], and other surface-treated materials [33] in hydrogels for improvements in strength but at the expense of economic and/or environmental cost. Recently, a significant amount of attention in biopolymer derived materials in adsorbent hydrogels has provided improved sustainability and excellent performance with a low carbon footprint [34]. Among different polymer backbone chemistries, polyacrylic acid chemistries are widely used in adsorption studies of cationic dyes [35]. Due to the presence of oxygen atoms, acrylics can complex cationic dyes. But a weak acidity of the carboxylic groups leaves these acrylic-based materials sensitive to solution pH, which affect dye adsorption capacity as a function of pH [25]. Novel adsorbents of the future should provide high adsorption capacity, low cost and effectiveness over a wide pH range.

Herein, we report a super-adsorbent hydrogel based on sodium styrene sulfonate monomer (NaSS). After producing a poly (NaSS) containing backbone with a strongly anionic polyelectrolyte results that provides negatively charged sulfonate groups along its backbone chain. These charges can be used for removal of cationic dyes like MB. An interesting feature of poly(NaSS) is that its pKa is approximately 1 [36], and hence, the sulfonate groups contribution towards swelling behavior is largely pH independent and increases the interaction strength with cationic dye moieties [37]. A low ionic pKa is a unique characteristic property making them ideal candidates to use in dye removal from wastewater streams under either acidic or alkaline conditions.

To improve the structural integrity and toughness of hydrogels for reusability, the polymer network was strengthened by copolymerizing NaSS and N, N′-dimethylacrylamide (DMA) monomers through crosslinking with a modified biopolymer, gelatin methacryloyl (GelMA) as crosslinker. DMA can induce additional self-crosslinking in the crosslinked polymer matrix, thereby increasing the porosity and available pore surface area for adsorption [38]. According to our knowledge, there are limited reports where NaSS was used as a monomer for hydrogel synthesis to be used as a dye-abatement adsorbent for methylene blue [39]. To date, most of the hydrogel adsorbents reported showing higher than 1000 mg/g adsorption capacities are based on advanced and expensive engineering materials such as graphene, carbon nanotubes [15,29,40] that compromise cost-effectiveness of an adsorption technique. The super-adsorbent hydrogels described herein demonstrated higher water absorption capacities with practical swelling ratios of over 27,500% that allow internal absorption sites to be fully exposed to MB, resulting in a high sorption capacity that reaches 1270 mg/g under neutral pH conditions.

A maximum adsorption of more than 1000 mg/g of MB by a NaSS-based super-adsorbent hydrogel is reported for the first time. A multilayer and heterogeneous adsorption of MB behavior by the super-adsorbent hydrogels that is supported by pseudo-first-order and Freundlich adsorption isotherm models is postulated. In addition, these super-adsorbent hydrogels demonstrate excellent regeneration capability, making them a promising and economically viable candidate for effective removal of organic dyes from wastewater.

2. Materials and Methods

2.1. Materials

Gelatin (type B, 100 bloom, from bovine skin), methacrylic anhydride, sodium carbonate, sodium bicarbonate, 2,2′-Azobis [2-(2-imidazolin-2-yl) propane] dihydrochloride (VA-044), sodium styrene sulfonate (NaSS), methylene blue (MB), sodium hydroxide (NaOH), hydrochloric acid (HCl), deuterium oxide (D_2O) were obtained from Sigma Aldrich and used as received. N, N′-dimethylacrylamide (DMA) monomers were passed through a basic alumina column prior to use. Ultra-high purity argon gas (99.999%) was obtained from Airgas.

2.2. Preparation of Gelatin Methacryloyl (GelMA)

GelMA was prepared using gelatin type B by following a procedure previously discussed by M Zhu et al. [41]. In brief, gelatin (20 g) was dissolved in 250 mL of carbonate-bicarbonate (CB) buffer (0.25 M) by continuous stirring at 50 °C maintained by water bath. The pH of the gelatin solution was adjusted to 9.4 using sodium hydroxide. Under vigorous stirring, methacrylic anhydride (0.1 mL per gram of gelatin) was slowly added and reaction continued for 2 h at 50 °C. The final pH of the reaction was adjusted to 7.4 to stop the reaction. The reaction mixture was filtered and then dialyzed against ultrapure water at 50 °C using a 12–14 kDa cutoff dialysis tubes, lyophilized, and stored at −20 °C until further use.

2.3. Preparation of Super-Adsorbent Hydrogels

The super-adsorbent hydrogel was prepared using a free radical polymerization technique in aqueous solution using a closed kettle reactor assembly as per our previously reported procedure [42]. A typical polymerization process is as follows: a GelMA solution (1% *w/v*) was prepared in 75 mL deionized water to which NaSS (13.5 g, 60 mol-% of total monomer) and DMA (4.34 g, 40 mol-% of total monomer) were added under argon gas and stirred until clear solution was obtained. Polymerization was initiated by adding VA-044 initiator (0.07 g, 0.2 mol-%) and reaction was continued for 24 h at 30 °C. The resulting hydrogel was cut in small cubes, dried at 60 °C in oven and pulverized before characterization and evaluation.

2.4. Physiochemical Characterization

Proton nuclear magnetic resonance spectroscopy (^1H NMR) spectroscopy (Bruker 400 MHz Avance III HD Liquid state NMR, Bruker, Switzerland) was used to quantify methacrylation of gelatin in D_2O. Fourier transform infrared spectroscopy (FT-IR) was used to examine the chemical structure of methacrylated gelatin and hydrogel samples. FT-IR spectra were recorded between 4000 and 400 cm^{-1} with setting of 16 signal-averaged scans at a resolution of 2 cm^{-1} using Nicolet iS50 FT-IR spectrometer (Thermo Fischer Scientific, Madison, WI, USA). The morphology and porous crosslinked polymer structure of the freeze-dried swollen hydrogel was studied using a high-resolution scanning electron microscope (Helios 600 Nanolab) at operating voltage of 5 kV. The samples were gold sputter-coated for charge dissipation. An elastic modulus of ~4 kPa for the as-synthesized gel of about 1 part gel per 4 parts water was measured using a Haake MARS III rheometer with a parallel plate geometry (PP35L Ti L) at 1 s^{-1}.

2.5. Swelling Measurements

The equilibrium swelling ratio of hydrogel was determined by immersing a weighed dried hydrogel sample in deionized water for 24 h. During this period water was changed every 8 h. The excess surface water on swollen gel was removed using filter paper and weight of swollen gel was taken. The equilibrium swelling ratio (ESR) was calculated using the Equation (1), where W_i is the initial mass of dried gel and W_f is the constant mass of swollen hydrogel at equilibrium. The temperature dependent equilibrium swelling

ratio was investigated by conducting swelling experiments at temperatures of 295, 305 and 315 K.

$$\text{Equilibrium Swelling Ratio (ESR)} = W_f/W_i \times 100\% \tag{1}$$

2.6. Dye Adsorption Studies

MB adsorption experiments applied water swollen super-adsorbent NaSS-DMA hydrogel as an adsorbent. MB stock solution of 100 ppm was prepared and further used to prepare MB solutions of different desired concentrations. A linear calibration curve of MB was constructed from absorbance measurements of 0.5, 1, 2, 3, 5, 8 and 10 ppm MB solutions. The absorbance was measured at the MB lambda maximum wavelength of 664 nm using absorbance spectra acquired in an Agilent Cary 60 UV-visible spectrometer (Agilent, Santa Clara, CA, USA) over the wavelength range of 400–800 nm.

The concentration of MB before and after adsorption were measured from absorption values further converted to concentration using linear calibration curve. The removal ratio ($R\%$) and the adsorption capacity (q_e) for MB were calculated using the Equations (2) and (3), where C_0 (mg/L), C_t (mg/L) and C_e (mg/L) are MB concentrations at initial time, time t, and equilibrium concentration respectively, V (L) is the volume of MB dye solution used and m (g) is the weight of dried adsorbent. All the experiments were carried out in triplicate and results represented here are the average of the three readings.

$$R\% = (C_0 - C_e)/C_0 \times 100\% \tag{2}$$

$$q_e = (C_0 - C_t) \times V/m \tag{3}$$

The effect of adsorbent dosage toward MB adsorption was investigated to set the adsorbent dose for rest of the adsorption experiments. Different adsorbent doses were added to 50 mL of MB solution of concentration 10 mg/L at 295 K and at a solution pH of 7.0. Incubator shaker under a constant speed of 100 rpm was used to maintain quality control of measurements. The final MB concentration was determined after 24 h of contact time.

For the effect of pH of MB solution on adsorption and removal of MB, 1 g of swollen hydrogel adsorbent was added into 50 mL of MB solution of concentration 50 mg/L at 295 K temperature. Initial pH of this solution was adjusted using 0.1 M HCl and 0.1 M NaOH in the range of 1 to 13. The final MB concentration was determined after 24 h of contact time.

For adsorption kinetics experiments, 1 g of swollen hydrogel adsorbent was added into 50 mL of MB solution of concentration 50 mg/L at 295 K temperature. A pH of 7.0 was found to provide optimum MB adsorption in early experiments of effect of solution pH. Concentration of MB in the solution was determined after designated time intervals. For adsorption isotherm and thermodynamic experiments, 1 g of swollen hydrogel adsorbent was added into MB solutions of different initial MB concentration with a solution pH of 7.0 and experiments were conducted at different temperatures (295 K, 305 K and 315 K). The final MB concentration was determined at 24 h of contact time.

2.7. Reusability

To investigate the reusability of the adsorbent, 1 g of swollen hydrogel adsorbent was added into 50 mL of MB solution of concentration 25 mg/L at 295 K temperature and pH of 7.0 to achieve saturated adsorption. Excess 0.1 M HCl was used to desorb MB that had adsorbed on hydrogel adsorbent [43]. The gel was regenerated in excess 0.1 M NaOH to regenerate anionic binding sites and finally washed with excess deionized water prior to use in the next adsorption cycle. An adsorption and desorption cycle was repeated four additional times using 50 mL of MB solution of concentration 25 mg/L at 295 K temperature and pH of 7.0.

3. Results and Discussion

3.1. Synthesis of Super-Adsorbent Hydrogel

In the present work, a super-adsorbent hydrogel was prepared via free radical polymerization of NaSS and DMA monomers employing GelMA as an organic crosslinker. A general synthesis scheme for the super-adsorbent hydrogel preparation is shown in Scheme 1. In the first step, GelMA was synthesized from gelatin, which is composed of diverse amino acids with hydroxyl and amino functionalities that can be modified into methacryloyl functionality by reacting with methacrylic anhydride in CB buffer [41]. In the second step, a single pot free radical polymerization was performed using aqueous soluble, VA-044 free radical initiator through a graft copolymerization technique.
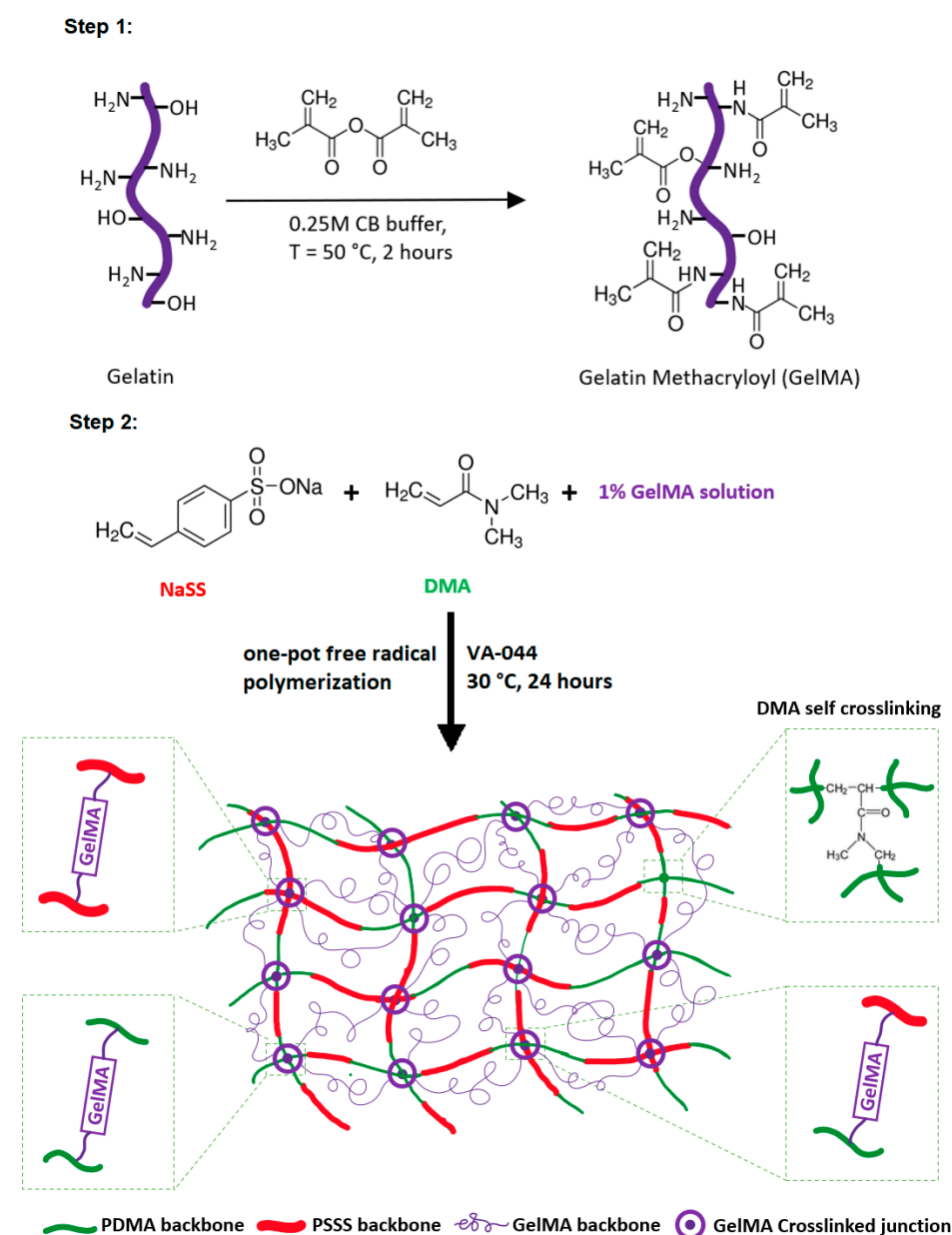
Scheme 1. Systematic synthesis of super-adsorbent hydrogels. Step 1: synthesis of gelatin methacryloyl (GelMA); Step 2: Free radical polymerization to obtain super-adsorbent hydrogel.

Figure 1a shows spectroscopic characterization of gelatin, GelMA and crosslinked superadsorbent hydrogel. The peaks at 3289 cm^{-1} (NH stretching), 2938 cm^{-1} (CH stretching), 1538 cm^{-1} (amide II), and an amide III bond present at 1238 cm^{-1}. These functional

groups are from the gelatin moiety of the GelMA product [44,45]. The peak around 1640 cm^{-1} in the spectrum of GelMA corresponds to the C=C stretching from the methacrylate functionalization, although amide I C=O stretching peak observed in the same region, making it difficult to distinguish. This observation is consistent with the previously reported literature [46]. The peaks near 1046 cm^{-1} are assigned as aliphatic ether C-O-C stretching due to the addition of the methacrylic moiety to gelatin, which confirms the functionalization [45]. A slight shift was observed of the broad band at 3300 cm^{-1}, which is characteristic of the N-H bond stretching vibration for N, N-substituted amides with addition of carboxylic hydroxyl [44]. The functionalization on gelatin was further confirmed by ^{1}H NMR spectroscopy as seen in Figure 1b.

In comparison between ^{1}H NMR spectrum of gelatin and GelMA, new proton peaks attributed to methacryloyl groups are detected between 5.1 to 5.7 ppm for vinyl protons (**CH$_2$**=C(CH$_3$)CONH–) of methacrylamide groups (Figure 1c) and at 1.8 ppm for methyl protons (CH$_2$=C(**CH$_3$**)CO–) of methacryloyl groups. As a result of functionalization, free lysine signal (NH$_2$**CH$_2$**CH$_2$CH$_2$CH$_2$–) of as such gelatin at 2.9 ppm was decreased significantly. Calculations based on NMR integration values indicate about 30% functionalization of free amino and hydroxyl groups. These results confirmed the successful functionalization of gelatin to GelMA and agreed well with previously reported studies [41,44,47].

The presence of NaSS-DMA copolymer in the synthesized hydrogel was confirmed with observed peaks corresponding to poly (NaSS) and poly (DMA) segments. Peak at 670 cm^{-1} for aromatic C–H out of plane bending vibration, 1010 and 1130 cm^{-1} for in-plane bending and in-plane skeleton vibrations of benzene ring, respectively corresponds to poly(NaSS) segment [48]. Additional absorptions at 1040 and 1180 cm^{-1} correspond to symmetric and asymmetric vibration absorption of SO$_3$$^-$ groups, respectively [48]. Absorption at 1615 cm^{-1} confirmed carbonyl stretching absorption by amide functionality present in the copolymer corresponding to the poly (DMA) segment [42,49]. The characteristic C–H bond from poly(DMA) units at around 2920 cm^{-1} was observed for vibration due to CH$_3$ groups along with the band around 1500–1570 cm^{-1} corresponds to C–N bending. The OH stretching vibration in frequency range of 3000–3700 cm^{-1} corresponds to moisture absorption by hydrogel [48].

Figure 1. *Cont.*
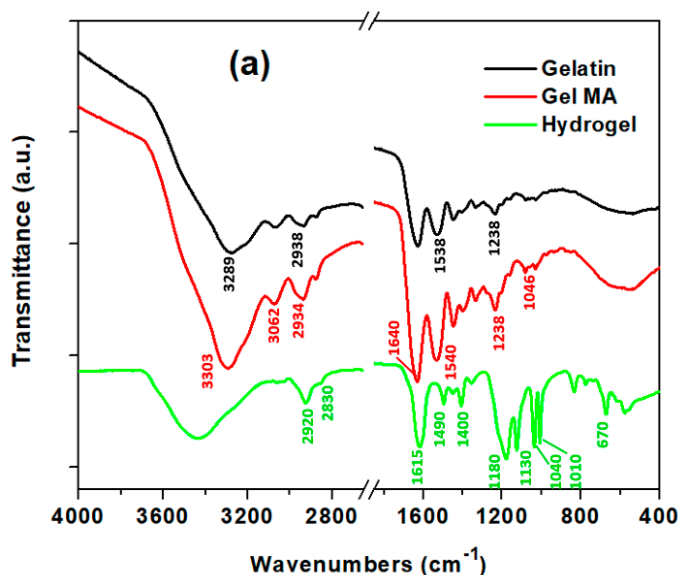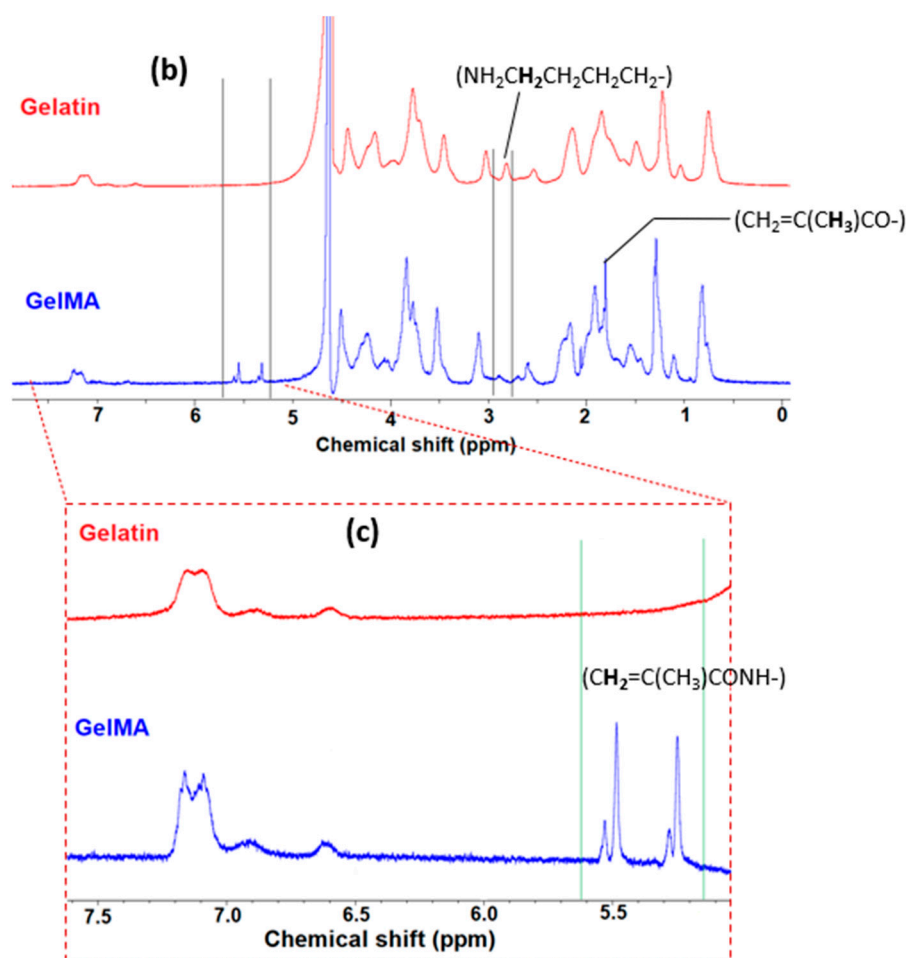
Figure 1. Spectroscopic characterization of gelatin, methacrylated gelatin (GelMA) and super-adsorbent hydrogel: (**a**) FT-IR, (**b**) ^{1}H NMR full spectra and (**c**) zoomed ^{1}H NMR spectra from 5.0 to 7.5 ppm.

3.2. Swelling of Super-Adsorbent Hydrogels

The water absorption capacity of a super-adsorbent hydrogel has an important effect on adsorption behavior for the removal of MB from aqueous solutions. A high swelling capacity can increase the available surface area for MB adsorption to aid improved adsorption capacity and removal efficiency [50]. Ionic polymers tend to show higher swelling capacities at the expense of weaker hydrogel integrity [51–53] causing them to fall apart during their use and contribute to significant material loss. To avoid this, these super-adsorbent hydrogels were synthesized as a copolymer of NaSS and DMA, which forms a tough, strong, crosslinked polymer network with GelMA.

The higher swelling ratios were observed that can reach up to 27,500% and above, which is higher than previously reported hydrogels synthesized using biopolymer based crosslinkers [54–56]. Figure 2a shows a pictorial representation of dry and swollen hydrogel that maintained structural integrity after complete swelling. As shown in Figure 2b, the SEM image of the freeze-dried swollen super-adsorbent hydrogel demonstrates a highly porous structure with average pore size of 0.91 ± 0.27 microns along with interconnected channels within pores. This internal porous structure is conducive to higher adsorption capacities. The extent of swelling ratio of super-adsorbent hydrogels at different temperatures is shown in Figure 2c. The swelling ratio of up to 28,760%, 28,220% and 27,760% was observed at 295 K, 305 K and 315 K respectively.
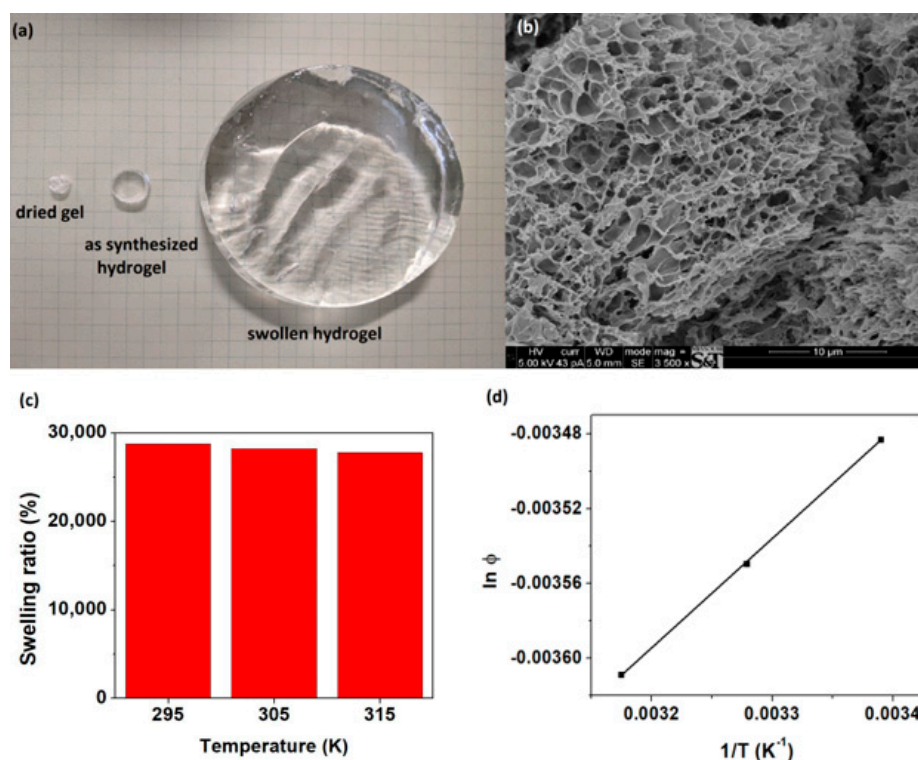
Figure 2. Swelling studies for super-adsorbent hydrogel. (**a**) pictorial representation of extents of swelling at 295 K in deionized water, (**b**) morphology and pore structure of the freeze-dried swollen super-adsorbent hydrogel, (**c**) equilibrium swelling ratio at different temperatures (295 K, 305 K and 315 K) and (**d**) van't Hoff analysis plot of ln Φ versus 1/T.

The thermodynamics of super-adsorbent hydrogel equilibrium swelling (EQSR) as a function of temperature using van't Hoff analysis was investigated. The change in enthalpy (ΔH) for super-adsorbent hydrogel can be calculated by the integrated van't Hoff equation:

$$\ln \Phi = -(\Delta H / 2.303 \, RT) + \text{constant} \tag{4}$$

where R = 8.314 J/(mol.K), T is the temperature (K) and $\Phi = 1 - (1/\text{EQSR})$ [57]. A linear plot of ln Φ versus 1/T as shown in Figure 2d, gives a linear fit with a slope of 0.5854 which is equal to $-(\Delta H / 2.303 \cdot R)$ from which the change in enthalpy (ΔH) of swelling process was calculated as −11.2087 kJ/mol. The negative change in enthalpy value suggests a fairly strong non-covalent bound-hydration and relaxation of polymer are occurring during the process of swelling and that a swollen state of the aqueous hydrogel is favored [58].

3.3. MB Dye Adsorption Studies

3.3.1. Effect of Adsorbent Dosage and pH

The dosage of adsorbent is an important parameter to adsorption behavior of hydrogel in removal of dyes from their aqueous solutions. MB adsorption capacity, q_e decreased with increasing adsorbent dose as seen in Figure 3, whereas the percent removal ratio remained nearly constant. A decrease in adsorption capacity can be attributed to the availability of adsorptive sites as a function of osmotic pressure. At higher dosages of adsorbent, adsorption will reach equilibrium quickly because of osmotic pressure and irrespective of unused active sites in comparison with lower dosages of adsorbent, which results in an efficient use of adsorption sites. The other extreme is at lower dosages of adsorbent, when used in higher concentration MB solutions, the adsorbent readily collapses resulting in poor adsorption removal capacity. Therefore, after comprehensive experimentation, a median dose of 1 g was selected for the remainder of adsorption experiments.
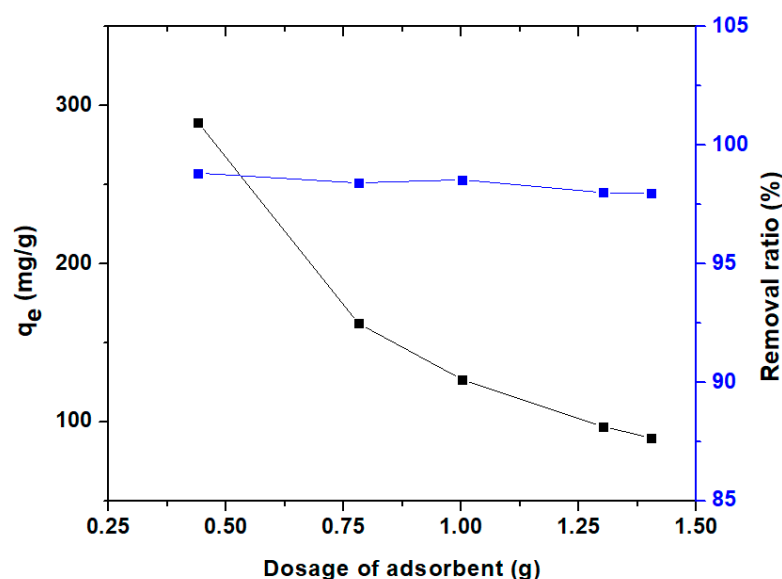
Figure 3. Effect of super-adsorbent gel dosage on adsorption capacity of MB and % removal ratio at 295 K, in MB solution with pH = 7.0, C_0 = 10 mg/L, after 24 h of contact.

Effect of pH of MB dye solution on adsorption capacity was investigated in MB solution of concentration 50 mg/L at 295 K as seen in Figure 4. The pH of dye solution did not show a significant effect on MB adsorption by super-adsorbent hydrogel, where >650 mg/g adsorption capacity was measured at pH = 7 with 99% removal ratio. A greater than 98% of MB removal ratio from aqueous dye solution on super-adsorbent hydrogel was measured at all pHs except at pH = 1, which showed a 87% removal ratio. The lower removal ratio can be attributed to the pH approaching the pK of the sulfonate group (pK~1.0) [54,59] that is responsible for the adsorption of MB via an ionic interaction between the adsorbent and cationic dye molecules. In strongly acidic solution, a competition for adsorption of dye moieties versus H^+ ions exists in addition to the H-bonding and charge-charge repulsion interactions between sulfonate groups from polymer and nitrogen units of MB with water. The competition causes a reduced adsorption capacity of adsorbent towards dye uptake in the strongly acidic solution.
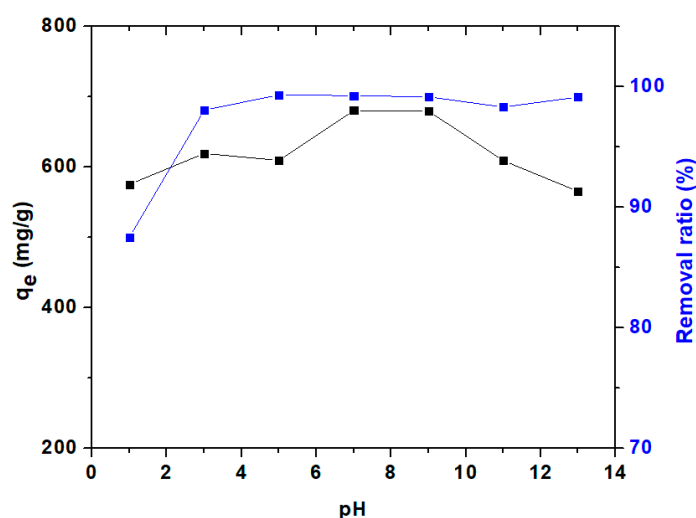

Figure 4. Effect of pH of MB dye solution on adsorption capacity q_e of MB and removal ratio at 295 K; MB solution with C_0 = 50 mg/L, dosage of hydrogel = 1 g; after 24 h of contact.

It was also observed that adsorption capacity increased slightly from pH 1 until pH 9 and then decreased upon a further increase in pH from 9 to 13. The observation indicates that the adsorption efficiency is also dependent on other physical adsorbant interactions besides electrostatic and hydrogen bonding. Under strongly acidic conditions of pH 1 and below, a decreased charge-charge attraction and thus a greater reliance on hydrogen bonding between the hydrogel adsorbent and MB is expected. On the other hand, in strongly alkaline conditions of pH > 10, a charge screening effect by excess Na^+ ions can also elicit a breakdown of hydrogen bonding interactions and cause the observed decrease in adsorption capacity. Overall, super-adsorbent hydrogel copolymers based on NaSS exhibit better adsorption of MB over a wide pH range of 2 to 12 compared to previously reported super-adsorbent hydrogels, which showed significant change in adsorption capacity as a function of pH [25].

3.3.2. Adsorption Kinetics

Adsorption kinetics is another important parameter as it provides important information about adsorption rate and adsorption mechanism. In general, the accepted mechanism for adsorption of dye involves several steps, including the following: penetration of dye molecules from solution into the adsorbent surface, diffusion of dye from the outer surface to internal adsorption sites, the interaction between dye molecules and the reactive sites present on polymer backbone through chemical bonding, electrostatic interactions, ion-exchange, hydrogen bonds, hydrophobic attractions, and so on [56,60–62]. The hydrogels discussed herein are based on NaSS, possessing aromatic side groups within the polymer backbone that can establish short range π-π interactions with aromatic groups present in MB. The NaSS structure thus presents not only sulfonate charge attraction but also π-π interactions that can result in stronger binding and increased adsorption capacity, as demonstrated in previous studies [16,63,64]. The effect of contact time on MB removal is shown in Figure 5, a typical adsorption capacity pattern increasing rapidly initially followed by an equilibrium as the adsorption sites are saturated. The adsorption equilibrium was achieved within 5 h contact time at 295 K in MB solution with C_0 = 50 mg/L, pH = 7.
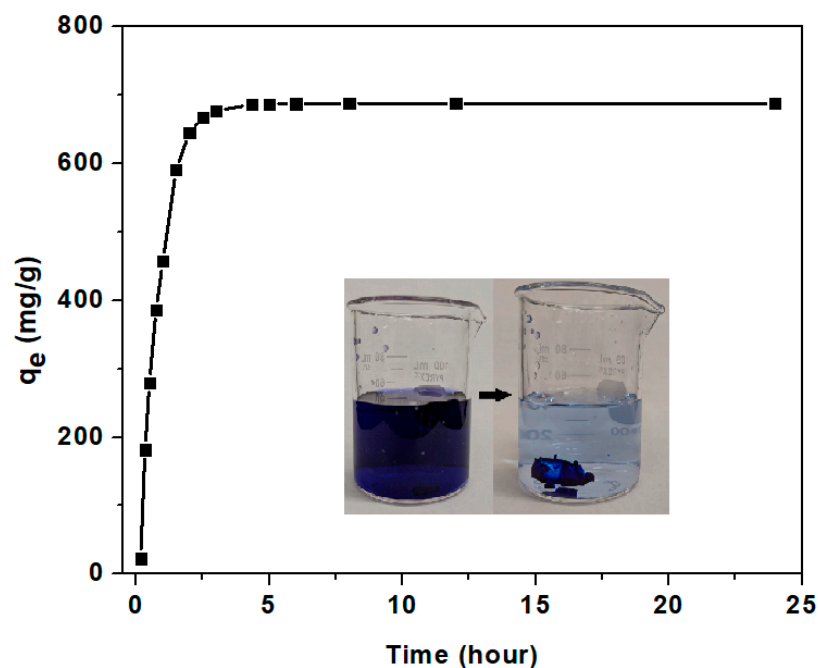

Figure 5. Adsorption of MB on super-adsorbent hydrogel as a function of time using MB solution at 295 K, with C_0 = 50 mg/L, pH = 7, dosage of super-adsorbent hydrogel = 1 g. Representation shows MB dye removal from solution.

To evaluate adsorption kinetics mechanisms and potential rate controlling steps, the experimental data were fitted to pseudo-first order (Equation (5)), pseudo-second order (Equation (6)), Boyd liquid-film diffusion model (Equation (7)), and Elovich models (Equation (8)) [65]

$$\log (q_e - q_t) = \log (q_e) - k_1 * t/2.303 \tag{5}$$

$$t/q_t = t/q_e + 1/(k_2 * q_e^2) \tag{6}$$

$$-\ln (1 - F) = k_{\text{fd}}t \tag{7}$$

$$q_t = ln(\alpha\beta)/\beta + lnt/\beta \tag{8}$$

where q_e (mg/g) and q_t (mg/g) are the adsorption capacity at equilibrium time and time t (min), respectively. k_1 (/min), pseudo first order rate constant, k_2 (g (mg/min)), pseudo second order rate constant, k_{fd} (/min) adsorption constant corresponding to Boyd liquid-film diffusion model, α (mg/g/min), initial adsorption rate constant and β (g/mg), desorption constant related to the adsorbent surface covering and the adsorption chemical energy. F is a fractional attainment of equilibrium ($F = q_t/q_e$) at time t for liquid-film diffusion. Based on the correlation coefficient (R^2), a best fit and most probable adsorption kinetics model for the adsorption was selected.

Each model was fitted with data obtained until time of equilibrium adsorption capacity attained (5 h) to avoid methodological bias of using q_t data at the equilibrium [66]. Plots are shown in Figure 6 and constants obtained from the plots summarized in Table 1. A pseudo-first-order model is based on the hypothesis that the rate of solute adsorption with time is proportional to the saturated concentration and number of unoccupied sites, whereas a pseudo-second-order model assumes that the adsorption rate is controlled by chemical adsorption through sharing or exchange of electrons between the adsorbent and adsorbate. The Elovich model, on the other hand, predicts multilayer adsorption where the rate of adsorption of solute decreases exponentially with the increase in the amount of adsorbed solute [67,68]. All three models are reaction-based models while the Boyd model is diffusion-based, which assumes that the boundary layer surrounding the adsorbent has the greatest effect on diffusion of solute and film diffusion is a rate limiting step during the initial phase of adsorption, followed by intraparticle diffusion [67,69,70].

Table 1. Kinetic parameters for MB adsorption on super-adsorbent hydrogels.

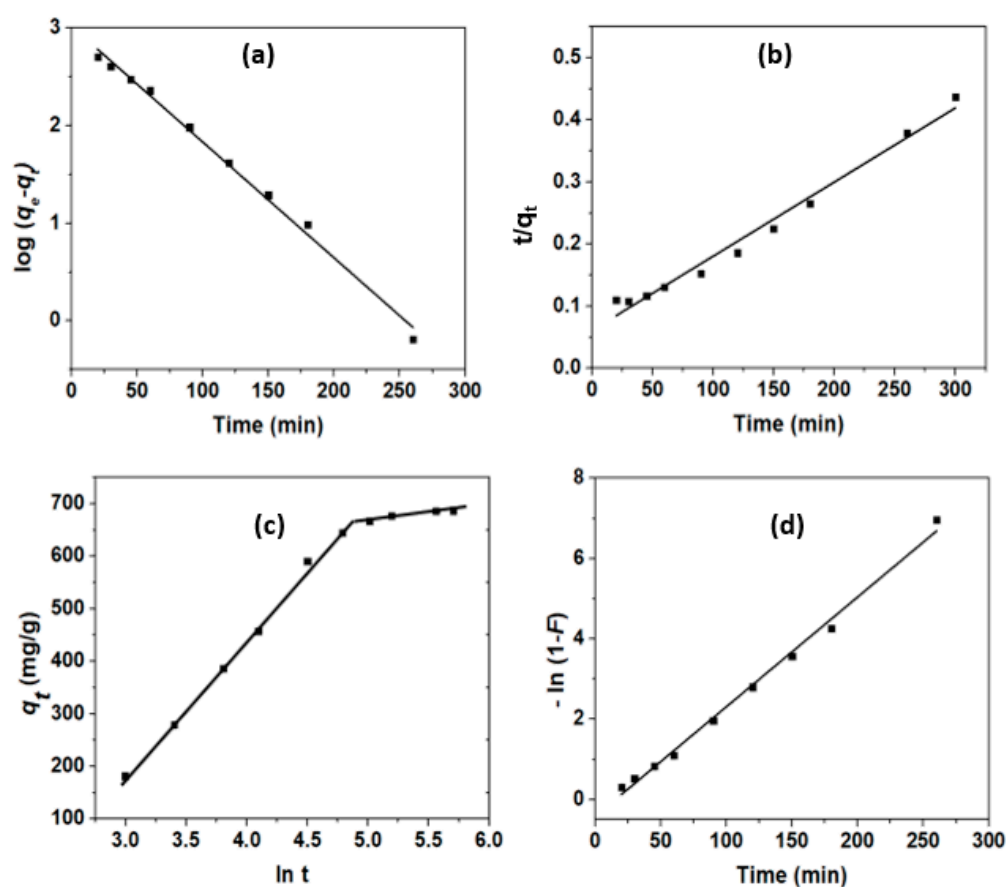| Pseudo-First-Order Model			
C_0 (mg/L)	q_e (mg/g)	k_1 (/min)	R^2
50	1048.14	0.0273	0.9933
Pseudo-second-order model			
C_0 (mg/L)	q_e (mg/g)	$k_2 \times 10^{-5}$ (/min)	R^2
50	833.33	2.3598	0.9813
Elovich model			
C_0 (mg/L)	α (mg/g/min)	β (g/mg)	R^2
50	31.0951	0.005	0.9323
Liquid film diffusion model			
C_0 (mg/L)	k_{fd} (/min)		R^2
50	0.02733		0.9933

Figure 6. Kinetic curves for (**a**) pseudo-first-order, (**b**) pseudo-second-order, (**c**) Elovich model and (**d**) Liquid film diffusion model on super-adsorbent hydrogel using MB solution at 295 K, with C_0 = 50 mg/L, pH = 7, dosage of super-adsorbent hydrogel = 1 g.

Based on correlation coefficient, a pseudo-first-order model was found to best represent the experimental data for adsorption of MB; thus, the rate-controlling step is ascribed to a number of unoccupied sites on super-adsorbent hydrogel. Moreover, according to an Elovich model, which shows two distinct linear regions, the adsorption process is found to be a multilayer and heterogeneous adsorption process. Where a liquid-film diffusion model was considered, a correlation coefficient R^2 of 0.9933 was observed that supports applicability of the model. The plot of $-(\ln(1 - F))$ versus time, however, did not pass through origin, implying that a liquid-film diffusion process was not the only rate-limiting step. The first linear portion of the plot $-(\ln(1 - F))$ versus time would be ascribed to surface diffusion, i.e., diffusion of MB from the bulk solution into the surface of super-adsorbent hydrogel, while the second linear portion would represent the gradual adsorption stage. In general, the whole process of adsorption of MB dye onto the super-adsorbent hydrogel involves multiple mechanisms, where π-π interactions, ion-exchange, hydrogen bonding, hydrophobic interactions, and liquid external diffusion are considered the main factors responsible for the observed adsorption capacities.

The effect of π-π interactions, aromatic hydrophobic interactions can be verified through proton NMR experiments (Figure S1, supplementary materials). Proton NMR demonstrated the broadening of signals for the MB protons associated with aromatic rings in the presence of aromatic polymer poly (NaSS), whereas no changes in proton signal broadening were observed in presence of poly (DMA) polymer. This is consistent with the previous reports focusing on aromatic π stackings interaction among aromatic dyes and aromatic polymers, by delocalization of aromatic π clouds leading to enhanced intermolecular electrostatic interactions [63,64,71].

3.3.3. Adsorption Isotherm Study

Figure 7 presents adsorption capacities of the super-adsorbent hydrogels as a function of temperature for MB adsorption at various initial concentrations of the MB solutions maintained at pH of 7.0. The lower initial concentration does not affect adsorption capacity significantly irrespective of temperature because of unsaturation of the adsorption sites. On the other hand, at higher initial MB concentration a temperature dependent adsorption phenomenon was observed where the active sites become saturated with dye molecules. With increase in temperature, a slight decrease in swelling ratio was observed, which will reduce bulk volume, pore volumes, and surface area available for adsorption [25,57,72]. As a result, adsorption capacity at 315 K was lower than at 295 K at highest initial MB concentrations. The q_e values thus depend on initial concentration of MB solution and other factors that determine the overall efficiency of the adsorption process.
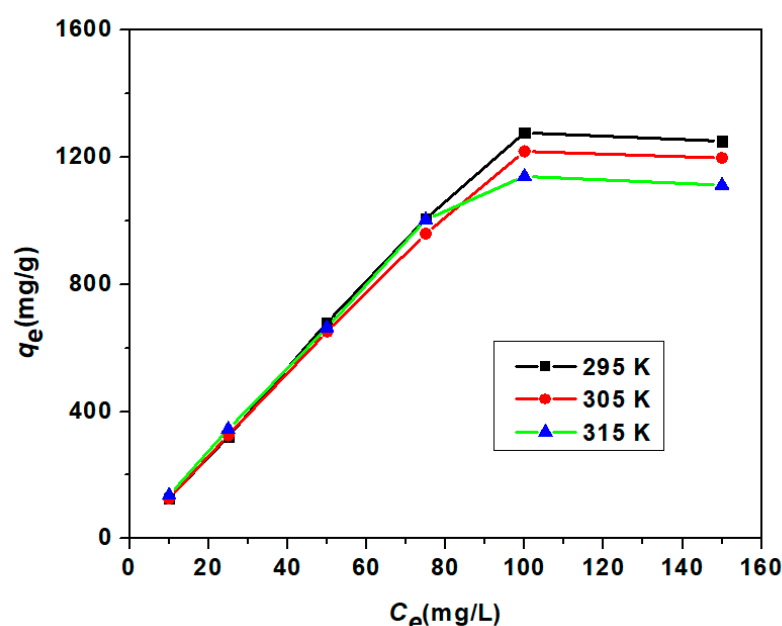

Figure 7. Effect of initial concentration of MB on adsorption capacity by super-adsorbent hydrogel as a function of concentration and temperature, pH = 7, dosage of super-adsorbent hydrogel = 1 g.

The adsorption capacity of the super-adsorbent hydrogels for MB adsorption was compared with other polymer systems reported in literature as shown in Table 2. This is the first report of a NaSS monomer based copolymer hydrogel adsorbent system, without expensive nanofiller, showing a greater than 1000 mg/g of adsorption capacities towards MB with value of 1270 mg/g.

For a better comprehension of the thermodynamics of MB adsorption on these super-adsorbent hydrogels, different adsorption isotherm equations of Langmuir, Freundlich and Temkin were examined at different temperatures (295 K, 305 K and 315 K) as a function of concentration. Adsorption isotherm study helps to describe the interaction of a dye molecule with adsorbent by providing a relationship between the concentration of dye in solution and an amount of dye adsorbed onto the hydrogel at equilibrium. The Langmuir isotherm is often applicable to a homogeneous adsorption surface with all the adsorption sites having equal adsorbate affinity, thus adsorbent-adsorbate intermolecular forces decrease quickly over time. The Freundlich isotherm is an empirical relationship for adsorption over heterogenous surfaces where adsorption occurs on a heterogeneous surface via multilayer adsorption with non-uniform heat of adsorption. On the other hand, the Temkin isotherm is based on the assumption that adsorption heat of all molecules decreases linearly as a function of increased coverage of the adsorbent surface where uniform distribution of binding energies can be expected.

Table 2. Comparison of maximum adsorption capacities for MB dye using adsorbent with variable chemical signature.

Adsorbent Chemical Signature	Adsorption Capacity (mg/g)	Reference
Poly (AA-co-VPA) hydrogel cross-linked with N-maleyl chitosan	66.89	[54]
Chitosan-crosslinked κ-carrageenan bionanocomposites	130.4	[55]
Tannic Acid–Poly (vinyl alcohol)/Sodium Alginate	147.06	[73]
PVA/carboxymethyl cellulose hydrogel	165.73	[74]
κ-Carrageenan/poly (glycidyl methacrylate) hydrogel	166.62	[56]
Amine functionalized sodium alginate hydrogel	400	[75]
Poly (acrylic acid) (PAA), cassava starch (CS) and poly (vinyl alcohol)	417	[76]
Poly (gellan gum-co-acrylamide-co-acrylic acid) hydrogel	423.46 ± 13.60	[77]
Gg-cl-P(AAm-co-MAA) hydrogel polymer	694.44	[78]
Cellulose/MMT	782.9	[33]
Xanthan gum-cl-poly (acrylic acid) based-reduced GO hydrogel	793.65	[40]
Sulfonate chitosan microspheres	820.1	[39]
Poly (sodium styrenesulfonate-co-dimethylacrylamide) crosslinked with gelatin methacryloyl	1270	[This work]
Poly (sodium styrene sulfonate) functionalized graphene (PSS-rGO)	1300	[29]

The equations used for Langmuir (Equation (9)), Freundlich (Equation (10)) and Temkin (Equation (11)) isotherms [79] are as follows:

$$C_e/q_e = C_e/q_m + 1/(K_L q_m) \tag{9}$$

$$ln\ q_e = ln\ K_F + ln\ C_e/n \tag{10}$$

$$q_e = B_T\ ln\ K_T + B_T\ ln\ C_e \tag{11}$$

where C_e (mg/L) is the equilibrium concentration of MB solution used; q_e (mg/g) is the adsorption capacity at equilibrium; q_m (mg/g) maximum adsorption capacity; K_L and K_F (L/mg) are the Langmuir and Freundlich adsorption equilibrium constants respectively; K_T (L/mg) is maximum binding energy constant; n is a heterogeneity factor indicating how favorable the adsorption process is; $B_T = RT/\beta$ and β (J/mol) is the Temkin constant related to the heat of adsorption, R is the universal gas constant (8.314 J/mol/); and T is absolute temperature (K).

Linear plots for each isotherm model are shown in Figure 8. The adsorption constants obtained from the plots associated with Langmuir, Freundlich and Temkin isotherm models are provided in Table 3. It is readily observed that the Freundlich model was best suited for MB adsorption to the hydrogel with R^2 values >0.99, which supports multilayer and heterogeneous adsorption process that was also supported by the Elovich kinetic modeling of Figure 6. The favorability and surface affinity for the adsorbate was investigated using n values which confirmed a transition of normal adsorption ($n > 1$) to cooperative adsorption ($n < 1$) as a function of decreasing temperature [79].

Table 3. Adsorption Isotherm Parameters for MB Adsorption on NaSS-DMA Hydrogels.

Model	Parameter	Unit	295 K	305 K	315 K
Langmuir Isotherm	q_m	mg/g	3861	3344.48	2439.02
	K_L	L/mg	0.00392	0.00454	0.00702
	R^2		0.5617	0.6528	0.7572

Table 3. *Cont.*

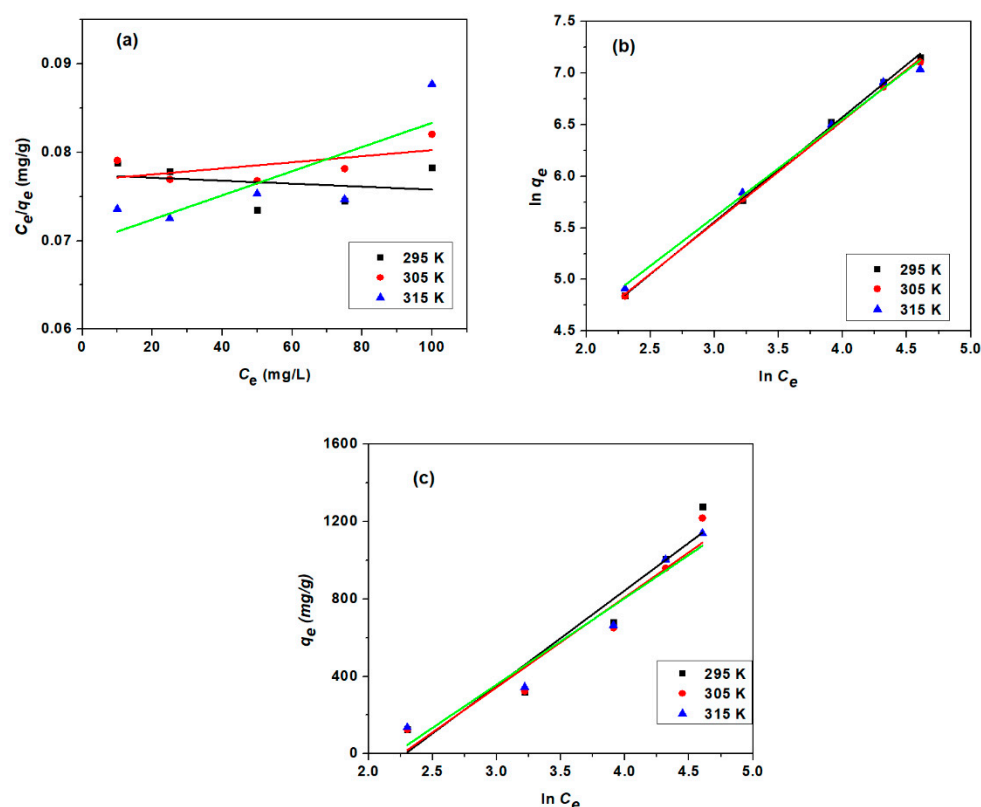| Model	Parameter	Unit	295 K	305 K	315 K
Freundlich Isotherm	n		0.9843	1.0095	1.0572
	K_F	L/mg	12.317	13.1713	15.9272
	R^2		0.9988	0.9989	0.994
Temkin Isotherm	β	J/mol	4.9755	5.2674	5.4859
	K_T	L/mg	0.1016	0.1041	0.1107
	R^2		0.902	0.9063	0.9295

Figure 8. Fitting curves of (**a**) the Langmuir isotherm model, (**b**) Freundlich isotherm model and (**c**) Temkin isotherm model for MB adsorption on super-adsorbent hydrogel at different temperatures using MB solutions at pH = 7 with dosage of super-adsorbent hydrogel = 1 g.

3.3.4. Thermodynamics of the Adsorption Process

In an adsorption process, standard enthalpy change, ΔH^0 (kJ/mol), standard entropy change, ΔS^0 (J/mol/K) and Gibbs free energy, ΔG^0 (kJ/mol), can be calculated for the adsorption isotherm to characterize the behavior of reaction and provide insight towards the favorability of adsorption process. The following Equations (11) and (12) can be used to calculate these thermodynamic parameters:

$$\Delta G^0 = -RT \, lnK_F \tag{12}$$

$$lnK_F = -(\Delta H^0)/RT + \Delta S^0/R \tag{13}$$

where R is the universal gas constant, 8.314 J/mol/K, T is absolute temperature (K), K_F is the Freundlich isotherm constant, which can be expressed as standard enthalpy and entropy changes of adsorption as functions of temperature. A plot of ln K_F versus 1/T can be used to determine the values of ΔH^0 and ΔS^0 from the slope and intercept [79].

Thermodynamic parameters were calculated for 295 K, 305 K and 315 K system temperatures where initial MB concentration was varied, as shown in Table 4. Negative values of Gibbs free energy interpret that the adsorption process was spontaneous at all the temperatures. Furthermore, a positive value of entropy change confirms spontaneity and a high level of (aqueous) disorder occurs in the adsorption process. A positive value of enthalpy change suggests that the adsorption process is endothermic in nature and driven by a strong entropy [80].

Table 4. Thermodynamic Parameters for Adsorption of MB onto NaSS-DMA Hydrogels.

Thermodynamic Parameters				
ΔG^0 (kJ/mol)			ΔH^0 (kJ/mol)	ΔS^0 (J/mol/K)
295 K	305 K	315 K		
−37.2	−38.6	−40.4	0.14	2.3

The thermodynamic parameters are attributed to the aromatic ring structures present in NaSS hydrogel polymer backbone and MB dye, which cause improved aggregation of aromatic groups and displacement of water of hydration from dye and polymer as a result of a hydrophobic planar stacking geometry. Release of surface-solvating water molecules would provide the favorable entropic and observed enthalpic contributions to the free energy. In addition to aqueous solvent contributions, site-specific interactions, such as short-range electrostatic interactions, hydrogen bond formation, π-π interaction other than aromatic, or cation-π interactions may also contribute to the free energy [16].

3.4. Recycalbility/Reusability of NaSS-DMA Super-Adsorbent Hydrogels

A capability to regenerate and reuse an adsorbent is a crucially important issue for an economic industrial application of adsorbent. The reusability of the NaSS-DMA copolymer hydrogel adsorbent was investigated over four repeat (five total) cycles of the adsorption–desorption-washing process, as shown in Figure 9. In the 4th repeat cycle, the adsorption capacity was 286 mg/g with a >90% removal efficiency, which supports the reusability of super-adsorbent hydrogels. A decrease in adsorption capacity in reuse is attributed to a partial, irreversible occupation of hydrogel active sites by MB dye molecules and a minimal mass loss of the hydrogel during the adsorption, desorption, and washing cyclic processing.
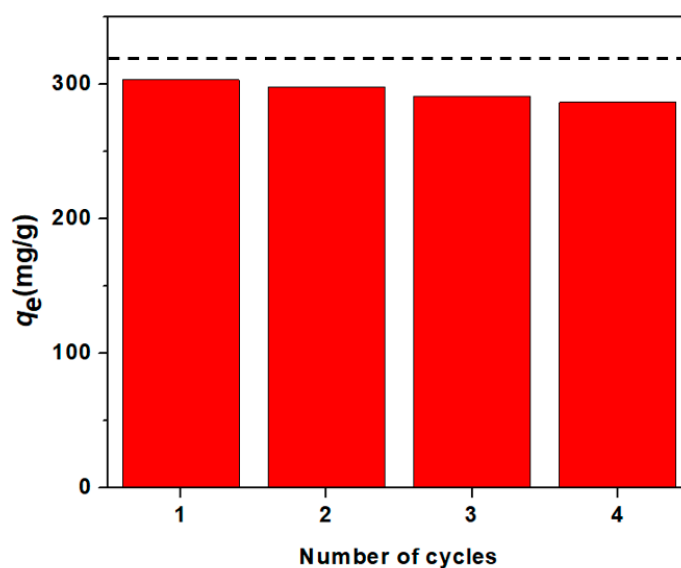

Figure 9. Reusability results for NaSS-DMA copolymer hydrogel for MB adsorption capacity at 295 K in MB solution at pH = 7.0, C_0 = 25 mg/L, and adsorbent dosage = 1 g. A dashed line represents original adsorption capacity before repeating adsorption-desorption cycles.

4. Conclusions

A super-adsorbent copolymer hydrogel based on NaSS and DMA monomers was synthesized using a single-step, bulk free radical polymerization using a lab synthesized GelMA organic crosslinker. Incorporation of GelMA created a well-crosslinked, tough polymer network that maintained hydrogel integrity even at very high equilibrium swelling ratios of up to 27,500%, which is an important aspect for reusability of hydrogels as adsorbent. Aromatic rings present in the polymer backbone structure enhance aromatic π-π interactions with MB dye that result in an improved adsorption capacity. The adsorption of MB to NaSS-DMA hydrogel is a complex process involving several mechanisms, where heterogenous and multilayer adsorption occurs as described by Elovich kinetics and Freundlich isotherm with a high adsorption capacity for MB dye, reaching upwards of 1270 mg/g. After 4 repeated cycles of desorption-adsorption, the hydrogel maintained structural integrity along with good adsorption performance with more than >90% removal efficiency that supports its use as a high-performance, recyclable adsorbent in industrial remediation applications. As a first report, NaSS copolymer-based hydrogels of high adsorption capacities towards cationic contaminants is a new approach toward high performance, super-adsorbent hydrogel adsorbent wastewater treatments.

References

1. Sokolowska-Gajda, J.; Freeman, H.S.; Reife, A. Synthetic dyes based on environmental considerations. Part 2: Iron complexes formazan dyes. *Dye Pigment* **1996**, *30*, 1–20. [CrossRef]
2. Methneni, N.; Morales-González, J.A.; Jaziri, A.; Mansour, H.B.; Fernandez-Serrano, M. Persistent organic and inorganic pollutants in the effluents from the textile dyeing industries: Ecotoxicology appraisal via a battery of biotests. *Environ. Res.* **2021**, *196*, 110956. [CrossRef]
3. Kabdaşli, I.; Tünay, O.; Orhon, D. Wastewater control and management in a leather tanning district. *Water Sci. Technol.* **1999**, *40*, 261–267. [CrossRef]
4. Farhan Hanafi, M.; Sapawe, N. A review on the water problem associate with organic pollutants derived from phenol, methyl orange, and remazol brilliant blue dyes. *Mater. Today Proc.* **2021**, *31*, A141–A150. [CrossRef]
5. Bohgard, M.; Ekholm, A.K. A method for the characterization of the aerosols emitted from handling of dye pigments in the paint manufacturing industry. *J. Aerosol Sci.* **1990**, *21*, S733–S736. [CrossRef]
6. Kaur, B.; Bhattacharya, S.N. 7—Automotive dyes and pigments. In *Handbook of Textile and Industrial Dyeing*; Clark, M., Ed.; Woodhead Publishing: Sawston, UK, 2011; Volume 2, pp. 231–251.
7. Wainwright, M. 6—Dyes for the medical industry. In *Handbook of Textile and Industrial Dyeing*; Clark, M., Ed.; Woodhead Publishing: Sawston, UK, 2011; Volume 2, pp. 204–230.
8. Hefford, R.J.W. 5—Colourants and dyes for the cosmetics industry. In *Handbook of Textile and Industrial Dyeing*; Clark, M., Ed.; Woodhead Publishing: Sawston, UK, 2011; Volume 2, pp. 175–203.

9.   Rafatullah, M.; Sulaiman, O.; Hashim, R.; Ahmad, A. Adsorption of methylene blue on low-cost adsorbents: A review. *J. Hazard. Mater.* **2010**, *177*, 70–80. [CrossRef] [PubMed]

10. Sinha, V.; Chakma, S. Advances in the preparation of hydrogel for wastewater treatment: A concise review. *J. Environ. Chem. Eng.* **2019**, *7*, 103295. [CrossRef]

11. Varjani, S.; Rakholiya, P.; Shindhal, T.; Shah, A.V.; Ngo, H.H. Trends in dye industry effluent treatment and recovery of value added products. *J. Water Process. Eng.* **2021**, *39*, 101734. [CrossRef]

12. Yagub, M.T.; Sen, T.K.; Afroze, S.; Ang, H.M. Dye and its removal from aqueous solution by adsorption: A review. *Adv. Colloid Interface Sci.* **2014**, *209*, 172–184. [CrossRef]

13. Gupta, V.K.; Pathania, D.; Agarwal, S.; Singh, P. Adsorptional photocatalytic degradation of methylene blue onto pectin–CuS nanocomposite under solar light. *J. Hazard. Mater.* **2012**, *243*, 179–186. [CrossRef]

14. Banat, I.M.; Nigam, P.; Singh, D.; Marchant, R. Microbial decolorization of textile-dyecontaining effluents: A review. *Bioresour. Technol.* **1996**, *58*, 217–227. [CrossRef]

15. Makhado, E.; Pandey, S.; Nomngongo, P.N.; Ramontja, J. Preparation and characterization of xanthan gum-cl-poly(acrylic acid)/o-MWCNTs hydrogel nanocomposite as highly effective re-usable adsorbent for removal of methylene blue from aqueous solutions. *J. Colloid Interface Sci.* **2018**, *513*, 700–714. [CrossRef] [PubMed]

16. Moreno-Villoslada, I.; González, R.; Hess, S.; Rivas, B.L.; Shibue, T.; Nishide, H. Complex Formation between Rhodamine B and Poly(sodium 4-styrenesulfonate) Studied by 1H-NMR. *J. Phys. Chem. B* **2006**, *110*, 21576–21581. [CrossRef]

17. Guimarães, J.R.; Guedes Maniero, M.; Nogueira de Araújo, R. A comparative study on the degradation of RB-19 dye in an aqueous medium by advanced oxidation processes. *J. Environ. Manag.* **2012**, *110*, 33–39. [CrossRef]

18. Zhang, M.; Gong, J.; Zeng, G.; Zhang, P.; Song, B.; Cao, W.; Liu, H.; Huan, S. Enhanced degradation performance of organic dyes removal by bismuth vanadate-reduced graphene oxide composites under visible light radiation. *Colloids Surf. A Physicochem. Eng. Asp.* **2018**, *559*, 169–183. [CrossRef]

19. Shalla, A.H.; Bhat, M.A.; Yaseen, Z. Hydrogels for removal of recalcitrant organic dyes: A conceptual overview. *J. Environ. Chem. Eng.* **2018**, *6*, 5938–5949. [CrossRef]

20. Pereira, A.G.B.; Rodrigues, F.H.A.; Paulino, A.T.; Martins, A.F.; Fajardo, A.R. Recent advances on composite hydrogels designed for the remediation of dye-contaminated water and wastewater: A review. *J. Clean. Prod.* **2021**, *284*, 124703. [CrossRef]

21. Labanda, J.; Sabaté, J.; Llorens, J. Modeling of the dynamic adsorption of an anionic dye through ion-exchange membrane adsorber. *J. Membr. Sci.* **2009**, *340*, 234–240. [CrossRef]

22. Mu, B.; Wang, A. Adsorption of dyes onto palygorskite and its composites: A review. *J. Environ. Chem. Eng.* **2016**, *4*, 1274–1294. [CrossRef]

23. Muya, F.N.; Sunday, C.E.; Baker, P.; Iwuoha, E. Environmental remediation of heavy metal ions from aqueous solution through hydrogel adsorption: A critical review. *Water Sci. Technol.* **2015**, *73*, 983–992. [CrossRef]

24. Zhao, S.; Zhou, F.; Li, L.; Cao, M.; Zuo, D.; Liu, H. Removal of anionic dyes from aqueous solutions by adsorption of chitosan-based semi-IPN hydrogel composites. *Compos. Part B Eng.* **2012**, *43*, 1570–1578. [CrossRef]

25. Hu, X.-S.; Liang, R.; Sun, G. Super-adsorbent hydrogel for removal of methylene blue dye from aqueous solution. *J. Mater. Chem. A* **2018**, *6*, 17612–17624. [CrossRef]

26. Le, H.Q.; Sekiguchi, Y.; Ardiyanta, D.; Shimoyama, Y. CO2-Activated Adsorption: A New Approach to Dye Removal by Chitosan Hydrogel. *ACS Omega* **2018**, *3*, 14103–14110. [CrossRef]

27. Kim, S.; Park, C.; Kim, T.-H.; Lee, J.; Kim, S.-W. COD reduction and decolorization of textile effluent using a combined process. *J. Biosci. Bioeng.* **2003**, *95*, 102–105. [CrossRef]

28. Gad, Y.H.; Aly, R.O.; Abdel-Aal, S.E. Synthesis and characterization of Na-alginate/acrylamide hydrogel and its application in dye removal. *J. Appl. Polym. Sci.* **2011**, *120*, 1899–1906. [CrossRef]

29. Hong, M.; Wang, Y.; Wang, R.; Sun, Y.; Yang, R.; Qu, L.; Li, Z. Poly(sodium styrene sulfonate) functionalized graphene as a highly efficient adsorbent for cationic dye removal with a green regeneration strategy. *J. Phys. Chem. Solids* **2021**, *152*, 109973. [CrossRef]

30. Mallakpour, S.; Rashidimoghadam, S. Poly(vinyl alcohol)/Vitamin C-multi walled carbon nanotubes composites and their applications for removal of methylene blue: Advanced comparison between linear and nonlinear forms of adsorption isotherms and kinetics models. *Polymer* **2019**, *160*, 115–125. [CrossRef]

31. Mallakpour, S.; Behranvand, V.; Mallakpour, F. Adsorptive performance of alginate/carbon nanotube-carbon dot-magnesium fluorohydroxyapatite hydrogel for methylene blue-contaminated water. *J. Environ. Chem. Eng.* **2021**, *9*, 105170. [CrossRef]

32. Bhattacharyya, A.; Ghorai, S.; Rana, D.; Roy, I.; Sarkar, G.; Saha, N.R.; Orasugh, J.T.; De, S.; Sadhukhan, S.; Chattopadhyay, D. Design of an efficient and selective adsorbent of cationic dye through activated carbon—Graphene oxide nanocomposite: Study on mechanism and synergy. *Mater. Chem. Phys.* **2021**, *260*, 124090. [CrossRef]

33. Peng, N.; Hu, D.; Zeng, J.; Li, Y.; Liang, L.; Chang, C. Superabsorbent Cellulose–Clay Nanocomposite Hydrogels for Highly Efficient Removal of Dye in Water. *ACS Sustain. Chem. Eng.* **2016**, *4*, 7217–7224. [CrossRef]

34. Zubair, M.; Ullah, A. Chapter 14—Biopolymers in environmental applications: Industrial wastewater treatment. In *Biopolymers and Their Industrial Applications*; Thomas, S., Gopi, S., Amalraj, A., Eds.; Elsevier: Amsterdam, The Netherlands, 2021; pp. 331–349.

35. Mohammadzadeh Pakdel, P.; Peighambardoust, S.J. A review on acrylic based hydrogels and their applications in wastewater treatment. *J. Environ. Manag.* **2018**, *217*, 123–143. [CrossRef]

36. Li, L.; Ferng, L.; Wei, Y.; Yang, C.; Ji, H.-F. Effects of acidity on the size of polyaniline-poly(sodium 4-styrenesulfonate) composite particles and the stability of corresponding colloids in water. *J. Colloid Interface Sci.* **2012**, *381*, 11–16. [CrossRef]

37. Kabiri, K.; Zohuriaan-Mehr, M.J.; Mirzadeh, H.; Kheirabadi, M. Solvent-, ion- and pH-specific swelling of poly(2-acrylamido-2-methylpropane sulfonic acid) superabsorbing gels. *J. Polym. Res.* **2010**, *17*, 203–212. [CrossRef]

38. Cipriano, B.H.; Banik, S.J.; Sharma, R.; Rumore, D.; Hwang, W.; Briber, R.M.; Raghavan, S.R. Superabsorbent Hydrogels That Are Robust and Highly Stretchable. *Macromolecules* **2014**, *47*, 4445–4452. [CrossRef]

39. Shi, H.; Dong, C.; Yang, Y.; Han, Y.; Wang, F.; Wang, C.; Men, J. Preparation of sulfonate chitosan microspheres and study on its adsorption properties for methylene blue. *Int. J. Biol. Macromol.* **2020**, *163*, 2334–2345. [CrossRef] [PubMed]

40. Makhado, E.; Pandey, S.; Ramontja, J. Microwave assisted synthesis of xanthan gum-cl-poly (acrylic acid) based-reduced graphene oxide hydrogel composite for adsorption of methylene blue and methyl violet from aqueous solution. *Int. J. Biol. Macromol.* **2018**, *119*, 255–269. [CrossRef] [PubMed]

41. Zhu, M.; Wang, Y.; Ferracci, G.; Zheng, J.; Cho, N.-J.; Lee, B.H. Gelatin methacryloyl and its hydrogels with an exceptional degree of controllability and batch-to-batch consistency. *Sci. Rep.* **2019**, *9*, 6863. [CrossRef]

42. Salunkhe, B.; Schuman, T.; Al Brahim, A.; Bai, B. Ultra-high temperature resistant preformed particle gels for enhanced oil recovery. *Chem. Eng. J.* **2021**, *426*, 130712. [CrossRef]

43. Bekiari, V.; Sotiropoulou, M.; Bokias, G.; Lianos, P. Use of poly(N,N-dimethylacrylamide-co-sodium acrylate) hydrogel to extract cationic dyes and metals from water. *Colloids Surf. A Physicochem. Eng. Asp.* **2008**, *312*, 214–218. [CrossRef]

44. Ruiz, C.; Vera, M.; Rivas, B.L.; Sánchez, S.; Urbano, B.F. Magnetic methacrylated gelatin-g-polyelectrolyte for methylene blue sorption. *RSC Adv.* **2020**, *10*, 43799–43810. [CrossRef]

45. Da Silva, K.; Kumar, P.; van Vuuren, S.F.; Pillay, V.; Choonara, Y.E. Three-Dimensional Printability of an ECM-Based Gelatin Methacryloyl (GelMA) Biomaterial for Potential Neuroregeneration. *ACS Omega* **2021**, *6*, 21368–21383. [CrossRef] [PubMed]

46. Fonseca, D.F.S.; Costa, P.C.; Almeida, I.F.; Dias-Pereira, P.; Correia-Sá, I.; Bastos, V.; Oliveira, H.; Vilela, C.; Silvestre, A.J.D.; Freire, C.S.R. Swellable Gelatin Methacryloyl Microneedles for Extraction of Interstitial Skin Fluid toward Minimally Invasive Monitoring of Urea. *Macromol. Biosci.* **2020**, *20*, 2000195. [CrossRef]

47. Shirahama, H.; Lee, B.H.; Tan, L.P.; Cho, N.-J. Precise Tuning of Facile One-Pot Gelatin Methacryloyl (GelMA) Synthesis. *Sci. Rep.* **2016**, *6*, 31036. [CrossRef] [PubMed]

48. Yang, J.C.; Jablonsky, M.J.; Mays, J.W. NMR and FT-IR studies of sulfonated styrene-based homopolymers and copolymers. *Polymer* **2002**, *43*, 5125–5132. [CrossRef]

49. Alpaslan, D.; Dudu, T.E.; Şahiner, N.; Aktas, N. Synthesis and preparation of responsive poly(Dimethyl acrylamide/gelatin and pomegranate extract) as a novel food packaging material. *Mater. Sci. Eng. C* **2020**, *108*, 110339. [CrossRef] [PubMed]

50. Zdravković, A.; Nikolić, L.; Ilić-Stojanović, S.; Nikolić, V.; Najman, S.; Mitić, Ž.; Ćirić, A.; Petrović, S. The removal of heavy metal ions from aqueous solutions by hydrogels based on N-isopropylacrylamide and acrylic acid. *Polym. Bull.* **2018**, *75*, 4797–4821. [CrossRef]

51. Rubinstein, M.; Colby, R.H.; Dobrynin, A.V.; Joanny, J.-F. Elastic Modulus and Equilibrium Swelling of Polyelectrolyte Gels. *Macromolecules* **1996**, *29*, 398–406. [CrossRef]

52. Koda, T.; Dohi, S.; Tachi, H.; Suzuki, Y.; Kojima, C.; Matsumoto, A. One-Shot Preparation of Polyacrylamide/Poly(sodium styrenesulfonate) Double-Network Hydrogels for Rapid Optical Tissue Clearing. *ACS Omega* **2019**, *4*, 21083–21090. [CrossRef]

53. Brannon-Peppas, L.; Peppas, N.A. Equilibrium swelling behavior of pH-sensitive hydrogels. *Chem. Eng. Sci.* **1991**, *46*, 715–722. [CrossRef]

54. Nakhjiri, M.T.; Marandi, G.B.; Kurdtabar, M. Poly(AA-co-VPA) hydrogel cross-linked with N-maleyl chitosan as dye adsorbent: Isotherms, kinetics and thermodynamic investigation. *Int. J. Biol. Macromol.* **2018**, *117*, 152–166. [CrossRef]

55. Mahdavinia, G.R.; Mosallanezhad, A. Facile and green rout to prepare magnetic and chitosan-crosslinked κ-carrageenan bionanocomposites for removal of methylene blue. *J. Water Process. Eng.* **2016**, *10*, 143–155. [CrossRef]

56. Lapwanit, S.; Sooksimuang, T.; Trakulsujaritchok, T. Adsorptive removal of cationic methylene blue dye by kappa-carrageenan/poly(glycidyl methacrylate) hydrogel beads: Preparation and characterization. *J. Environ. Chem. Eng.* **2018**, *6*, 6221–6230. [CrossRef]

57. Xiang, T.; Lu, T.; Zhao, W.-F.; Zhao, C.-S. Ionic-Strength Responsive Zwitterionic Copolymer Hydrogels with Tunable Swelling and Adsorption Behaviors. *Langmuir* **2019**, *35*, 1146–1155. [CrossRef] [PubMed]

58. Safronov, A.P.; Smirnova, Y.A.; Pollack, G.H.; Blyakhman, F.A. Enthalpy of Swelling of Potassium Polyacrylate and Polymethacrylate Hydrogels. Evaluation of Excluded-Volume Interaction. *Macromol. Chem. Phys.* **2004**, *205*, 1431–1438. [CrossRef]

59. Lewis, S.R.; Datta, S.; Gui, M.; Coker, E.L.; Huggins, F.E.; Daunert, S.; Bachas, L.; Bhattacharyya, D. Reactive nanostructured membranes for water purification. *Proc. Natl. Acad. Sci. USA* **2011**, *108*, 8577–8582. [CrossRef]

60. Dąbrowski, A. Adsorption—From theory to practice. *Adv. Colloid Interface Sci.* **2001**, *93*, 135–224. [CrossRef]

61. Noroozi, B.; Sorial, G.A. Applicable models for multi-component adsorption of dyes: A review. *J. Environ. Sci.* **2013**, *25*, 419–429. [CrossRef]

62. Melo, B.C.; Paulino, F.A.A.; Cardoso, V.A.; Pereira, A.G.B.; Fajardo, A.R.; Rodrigues, F.H.A. Cellulose nanowhiskers improve the methylene blue adsorption capacity of chitosan-g-poly(acrylic acid) hydrogel. *Carbohydr. Polym.* **2018**, *181*, 358–367. [CrossRef]

63. Moreno-Villoslada, I.; Torres, C.; González, F.; Shibue, T.; Nishide, H. Binding of Methylene Blue to Polyelectrolytes Containing Sulfonate Groups. *Macromol. Chem. Phys.* **2009**, *210*, 1167–1175. [CrossRef]

64. Moreno-Villoslada, I.; Jofré, M.; Miranda, V.; Chandía, P.; González, R.; Hess, S.; Rivas, B.L.; Elvira, C.; San Román, J.; Shibue, T.; et al. π-Stacking of rhodamine B onto water-soluble polymers containing aromatic groups. *Polymer* **2006**, *47*, 6496–6500. [CrossRef]

65. Lopičić, Z.R.; Stojanović, M.D.; Marković, S.B.; Milojković, J.V.; Mihajlović, M.L.; Kaluđerović Radoičić, T.S.; Kijevčanin, M.L.J. Effects of different mechanical treatments on structural changes of lignocellulosic waste biomass and subsequent Cu(II) removal kinetics. *Arab. J. Chem.* **2019**, *12*, 4091–4103. [CrossRef]

66. Simonin, J.-P. On the comparison of pseudo-first order and pseudo-second order rate laws in the modeling of adsorption kinetics. *Chem. Eng. J.* **2016**, *300*, 254–263. [CrossRef]

67. Kajjumba, G.W.; Emik, S.; Öngen, A.; Özcan, H.K.; Aydın, S. Modelling of Adsorption Kinetic Processes—Errors, Theory and Application. In *Modelling of Adsorption Kinetic Processes—Errors, Theory and Application, Advanced Sorption Process Applications*; Edebali, S., Ed.; IntechOpen: London, UK, 2019. [CrossRef]

68. León, G.; Saura, F.; Hidalgo, A.M.; Miguel, B. Activated Olive Stones as a Low-Cost and Environmentally Friendly Adsorbent for Removing Cephalosporin C from Aqueous Solutions. *Int. J. Environ. Res. Public Health* **2021**, *18*, 4489. [CrossRef] [PubMed]

69. Singh, S.K.; Townsend, T.G.; Mazyck, D.; Boyer, T.H. Equilibrium and intra-particle diffusion of stabilized landfill leachate onto micro- and meso-porous activated carbon. *Water Res.* **2012**, *46*, 491–499. [CrossRef] [PubMed]

70. Boyd, G.E.; Adamson, A.W.; Myers, L.S. The Exchange Adsorption of Ions from Aqueous Solutions by Organic Zeolites. II. Kinetics1. *J. Am. Chem. Soc.* **1947**, *69*, 2836–2848. [CrossRef]

71. Parenti, F.; Tassinari, F.; Libertini, E.; Lanzi, M.; Mucci, A. Π-Stacking Signature in NMR Solution Spectra of Thiophene-Based Conjugated Polymers. *ACS Omega* **2017**, *2*, 5775–5784. [CrossRef]

72. Yu, H.; Grainger, D.W. Thermo-sensitive swelling behavior in crosslinked N-isopropylacrylamide networks: Cationic, anionic, and ampholytic hydrogels. *J. Appl. Polym. Sci.* **1993**, *49*, 1553–1563. [CrossRef]

73. Hu, T.; Liu, Q.; Gao, T.; Dong, K.; Wei, G.; Yao, J. Facile Preparation of Tannic Acid–Poly(vinyl alcohol)/Sodium Alginate Hydrogel Beads for Methylene Blue Removal from Simulated Solution. *ACS Omega* **2018**, *3*, 7523–7531. [CrossRef]

74. Dai, H.; Huang, Y.; Huang, H. Eco-friendly polyvinyl alcohol/carboxymethyl cellulose hydrogels reinforced with graphene oxide and bentonite for enhanced adsorption of methylene blue. *Carbohydr. Polym.* **2018**, *185*, 1–11. [CrossRef]

75. Godiya, C.B.; Xiao, Y.; Lu, X. Amine functionalized sodium alginate hydrogel for efficient and rapid removal of methyl blue in water. *Int. J. Biol. Macromol.* **2020**, *144*, 671–681. [CrossRef]

76. Arayaphan, J.; Maijan, P.; Boonsuk, P.; Chantarak, S. Synthesis of photodegradable cassava starch-based double network hydrogel with high mechanical stability for effective removal of methylene blue. *Int. J. Biol. Macromol.* **2021**, *168*, 875–886. [CrossRef] [PubMed]

77. Zheng, M.; Cai, K.; Chen, M.; Zhu, Y.; Zhang, L.; Zheng, B. pH-responsive poly(gellan gum-co-acrylamide-co-acrylic acid) hydrogel: Synthesis, and its application for organic dye removal. *Int. J. Biol. Macromol.* **2020**, *153*, 573–582. [CrossRef] [PubMed]

78. Mittal, H.; Maity, A.; Ray, S.S. Effective removal of cationic dyes from aqueous solution using gum ghatti-based biodegradable hydrogel. *Int. J. Biol. Macromol.* **2015**, *79*, 8–20. [CrossRef] [PubMed]

79. Al-Ghouti, M.A.; Al-Absi, R.S. Mechanistic understanding of the adsorption and thermodynamic aspects of cationic methylene blue dye onto cellulosic olive stones biomass from wastewater. *Sci. Rep.* **2020**, *10*, 15928. [CrossRef] [PubMed]

80. Khajeh, M.; Dastafkan, K.; Bohlooli, M.; Ghaffari-Moghaddam, M. CHAPTER 10 Sample Preparation and Extraction Techniques Using Nanomaterials. In *Advanced Environmental Analysis: Applications of Nanomaterials*; The Royal Society of Chemistry: London, UK, 2017; Volume 1, pp. 221–283.